Oxygen vacancies induced ferromagnetism in undoped and Cr doped SnO_2 nanowires

Li Zhang*, Shihui Ge*, Yalu Zuo* and Jing Qing*
* Key Laboratory for Magnetism and Magnitic Materials of Ministry of Education,
Lanzhou University, Lanzhou 730000, P.R.China, gesh@ lzu.edu.cn

ABSTRACT

We presented detailed characterizations of the ferromagnetic properties of undoped and Cr-doped SnO_2 nanowires synthesized by chemical vapor deposition. All the samples exhibit room-temperature ferromagnetism. Our experiments reveal that, in addition to the contribution of surface oxygen vacancies, Cr doping into SnO_2 plays an important role in tuning the ferromagnetism of SnO_2 nanostructures. Doping the SnO_2 nanowires with 1.8at.% Cr enhances the magnetization by 28%. We applied the bound magnetic polaron model to successfully explain the enhancement of ferromagnetism.

Keywords: chemical vapor deposition (CVD), nanostructure, ferromagnetism, oxygen vacancies, bound magnetic polaron (BMP)

1 INTRODUCTION

Following the first discovery in Co-doped anatase TiO_2 thin film [1], significant work has shown that 3*d* transition-metal (TM)-doped semiconducting and insulating oxides such as ZnO, TiO_2 and SnO_2 [2-4], exhibit ferromagnetism (FM) above room temperature (RT), whose origin was primarily attributed to the doping. However, the finding of unexpected FM in HfO_2 thin films [5] has excited the revisit of the real role that a doping may play in tailoring the magnetic properties. The observations of FM in various pristine oxides such as TiO_2, In_2O_3, ZnO confirmed that magnetism is certainly possible in pure semiconducting and insulating oxides, where FM is attributed to the oxygen vacancies (OVs) or cation defects [6-8]. Recently, we have reported ferromagnetic properties in undoped SnO_2 nanowires prepared by chemical vapor deposition (CVD), and showed that the observed FM is likely due to the OVs at the surface [9]. However, the role of TM doping still remains unclear in these systems and there currently exist considerable debates in the literature [10-12]. In this paper, we present a detailed characterization of the magnetic properties of pristine and Cr-doped SnO_2 nanowire to investigate the role of a TM doping in tailoring FM. Unlike many other TM, Cr itself is antiferromagnetic and would not induce an extrinsic FM even if Cr clustering occurs. Moreover, trivalent Cr^{3+} ions exhibit $3d^3$ high-spin configuration, which helps to generate large magnetic moments in the host semiconductors [13]. Therefore, our system provides an excellent platform to conveniently investigate the origin of intrinsic FM.

2 EXPERIMENTAL METHODS

Our samples were synthesized with CVD method. To grow Cr-doped SnO_2 nanowires, highly pure Sn (99.9%) and $CrCl_3$ (99.9%) powders were mixed and ground thoroughly in a mortar. The mixture was loaded at a ceramic boat, which was located at the center of a quartz tube. The Si (100) substrates coated with 5 nm Au layers served as the catalyst positioned in the boat at an appropriate distance away from the source materials. The quartz tube was evacuated to a pressure of less than 2Pa and then heated to 900°C. A stable argon flow with a rate of 100 SCCM (SCCM denotes cubic centimeter per minuter at STP) was introduced into the quartz tube as the carrier gas during heating and cooling process. At 900°C, oxygen was introduced and the flux rate of argon was modulated to 30 SCCM; the process took 30 minutes, and the white material was formed on the surface of the substrates. In our work, $Sn_{1-x}Cr_xO_{2-\delta}$ nanowires with x=0.018, 0.048 and 0.072 were obtained by modulating the weight ratio of the Sn and $CrCl_3$ powders. For the synthesis of undoped SnO_2 nanowires, all the experimental conditions remained the same except that $CrCl_3$ was not used in the source powder.

The morphology and structure of the samples were characterized by scanning electron microscope (SEM) (Hitachi S-4800) and X-ray diffraction (XRD) (Philips X' Pert model). Further microstructural characterization was performed using high-resolution transmission electron microscope (HRTEM) (JEOL, JEM-2010 at 200 kV) imaging and selected area electron diffraction (SAED) pattern analysis. The magnetic properties of the samples were measured by a Quantum Design magnetometer (MPMS XL SQUID) from 5 to 305 K and a vibrating sample magnetometer (VSM) (LakeShore 7304 model) at RT. The chemical bonding states and the compositions of the products were determined by x-ray photoelectron spectroscopy (XPS) (a VG Scientific ESCALAB-210 spectrometer). Micro photoluminescence (PL) measurement were carried out at RT using a He-Cd laser with a wavelength of 325 nm as the excitation source.

Throughout all the experimental steps taken during synthesis and measurements, only high pure reagent, gas source and alumina boat were used. All the tools used for handing the samples were nonferromagnetic and plastic

based to avoid any unintentional contact with metals. Moreover, all the Si (100) substrates uncoated or coated with Au layers were measured under the same sequences as for the samples to examine the possible contamination contributing to the observed FM. All the substrates showed the expected diamagnetic behavior.

3 RESULTS AND DISCUSSION

Figure 1a shows the SEM images of the undoped SnO_2 sample. Clearly, all the products are in the form of nanowires, direction-free on the substrate with a high density. The SnO_2 nanowires are homogeneous with diameters around 50nm (Fig. 1a, inset) and length greater than 20 μm. Compared with the undoped SnO_2 nanowires, Cr doping does not change the morphology and all the products remain as nanowires. However, although each individual nanowire for all samples has a uniform diameter along its length (which reaches 15 μm), the nanowire diameters scatter between 50 and 100 nm (as seen in Fig. 1b for the $Sn_{0.982}Cr_{0.018}O_{2-\delta}$ nanowires), indicating the possible influence of Cr doping on the nanowire width. Figure 1c shows a catalyst cap on the tip of a nanowire with a size close to that of the nanowire, which evidences that the growth mechanism of SnO_2 nanowires in our experiment is the vapor–liquid–solid (VLS) mechanism [14].

The structural characteristics of the $Sn_{1-x}Cr_xO_{2-\delta}$ nanowires were investigated in detail by using TEM and HRTEM. Fig. 1d shows a typical TEM bright-field image of $Sn_{0.982}Cr_{0.018}O_{2-\delta}$ nanowires with a width ~ 70 nm, indicating the diameter uniformity along the nanowire length. A ripple-like contrast observed in the TEM image is due to the strain resulting from the bending of the nanowires. The HRTEM image shows that the nanowire is structurally uniform, and the clear lattice fringes illustrate that the nanowire is a single crystalline (Fig. 1e). The interplanar spacing is about 0.343 nm, which corresponds to the {110} plane of the rutile crystalline SnO_2, implying that the nanowires grow along <110> direction. The inset shows the SAED pattern that can be indexed on a tetragonal cell with lattice parameters of a=4.737 Å and c=3.185 Å, which further confirms that the nanowire is a single-crystal rutile SnO_2. No secondary phase or clusters were observed, verifying that Cr has been doped into SnO_2 lattice. The undoped SnO_2 nanowires have the same structures as Cr-doped SnO_2 nanowires.

Figure 1f shows XRD patterns of undoped SnO_2 nanowires and $Sn_{1-x}Cr_xO_{2-\delta}$ nanowires with x = 0.018, 0.048 and 0.072. For each sample, all observed peaks can be indexed with the rutile-type tetragonal structure of SnO_2 (JCPDS 21-1250), which are consistent with the standard values for bulk SnO_2. No characteristic peaks of impurities, such as other forms of tin oxides, pure Sn or Cr oxides, were observed within the detection sensitivity. Compared with the undoped SnO_2 nanowires, the diffraction peak position shifts to a larger angle with increased Cr content, revealing a possible change in lattice parameters. Such a change is quantified in Fig. 1g, where the lattice parameter *a* decreases monotonously with increased Cr content. The shrinkage of lattice constant after doping can be attributed to the substitution of the smaller Cr^{3+} ions (0.65 Å) onto the Sn^{4+} (0.69 Å) lattice sites [15], which indicates that Cr ions are incorporated into the SnO_2 matrix.

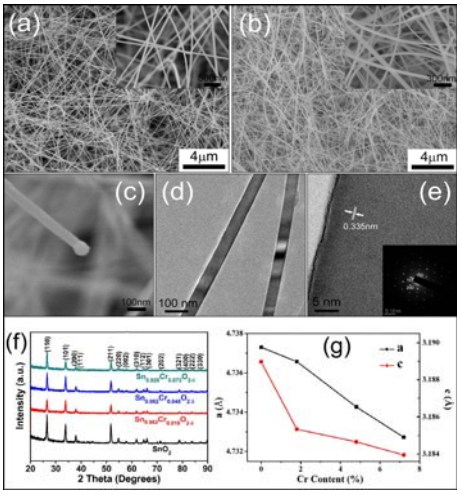

Figure 1. Low-magnification SEM images for (a) SnO_2 and (b) $Sn_{0.982}Cr_{0.018}O_{2-\delta}$ nanowires. (c) The end of an individual $Sn_{0.982}Cr_{0.018}O_{2-\delta}$ nanowire. (d) TEM image of $Sn_{0.982}Cr_{0.018}O_{2-\delta}$ nanowires. (e) HRTEM image and corresponding SAED pattern (inset) of $Sn_{0.982}Cr_{0.018}O_{2-\delta}$ nanowires. (f) XRD patterns of SnO_2 and $Sn_{1-x}Cr_xO_{2-\delta}$ nanowires with different x. (g) Evolution of the lattice parameters a and c as a function of Cr content *x*.

Further evidence for the purity and composition of the products were obtained by XPS, showing that no impurities were detected in all the samples within the detection limit. Two representative XPS spectra of the undoped SnO_2 and $Sn_{0.982}Cr_{0.018}O_{2-\delta}$ nanowires are shown in Fig. 2, where Figs. 2a –2c are the survey spectra, the Sn 2p, and O 1s core-level spectrum, respectively. The double spectral lines of Sn 3d appear at the binding energy of 486.6 eV (Sn $3d_{5/2}$) and 495 eV (Sn $3d_{3/2}$) with a spin-orbit splitting of 8.4 eV, which coincides with the findings for the Sn^{4+} bound to oxygen in the SnO_2 matrix [16]. The peak of Sn $3d_{5/2}$ shows only one symmetric component without a shoulder peak, indicating the absence of Sn^{2+} ions. On the other hand, an asymmetric O 1*s* peak is observed for the sample, which has a shoulder at the higher binding energy side. By fitting with Gaussian distributions, we obtained two peaks at 531 and 533 eV. The dominant one is located at 531 eV, which corresponds to the O 1s core peak of O^{2-} bound to Sn^{4+}, and normally assigned as the low binding energy component (LBEC). The peak at 533 eV is referred to as the high binding energy component (HBEC) [17]. We will discuss them in detail below. Moreover, as shown in the inset of Fig. 2a, the Cr $2p_{3/2}$ peak was detected at 577.5 eV for the $Sn_{0.982}Cr_{0.018}O_{2-\delta}$ sample, which matches that of Cr^{3+} ions

(577.2 eV) [18,19]. It confirms that Cr ions in our samples have a chemical valence of 3+.

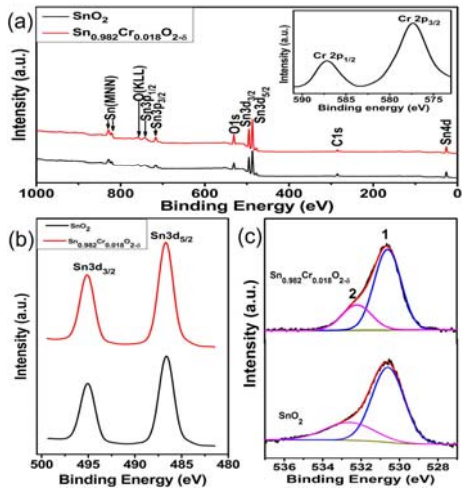

Figure 2. XPS spectra for SnO_2 and $Sn_{0.982}Cr_{0.018}O_{2-\delta}$ nanowires: (a) the survey spectra, (b)Sn 3*d*, (c)O1*s*. The inset of (a) is the detail scan of Cr $2p_{3/2}$ and $2p_{1/2}$ peaks for $Sn_{0.982}Cr_{0.018}O_{2-\delta}$.

Figure 3a shows the magnetic hysteresis (M-H) curves of all samples measured at RT, where the contributions from the diamagnetism of Si substrate and the paramagnetism (PM) of samples have been subtracted. All the samples are clearly ferromagnetic at RT and their loops have small coercivities in the range from 80 to 120 Oe. Note that the observed FM should be intrinsic in all samples, since the measurements above (HRTEM, SAED, XRD and XPS) did not detect the Sn-based binary, ternary oxide candidates, pure Sn clusters or Cr secondary phase.

A large special magnetization M of 0.081 emu/g is observed for the undoped SnO_2 nanowires, much larger than that of SnO_2 nanoparticles (<0.002emu/g) in Ref. [20]. Note that $Sn_{0.982}Cr_{0.018}O_{2-\delta}$ nanowires exhibits M of 0.104emu/g, larger than that of undoped SnO_2 nanowires, which decreases with further increased dopant concentration x (Fig. 3, inset). Clearly, doping with 1.8% of Cr can certainly enhance the magnetization of the pristine SnO_2 nanowires, implying additional contributions brought by Cr doping. Given that Cr^{3+} ions enter the SnO_2 lattice and substitute for Sn^{4+} ions, it infers that Cr doping generates additional OVs which might be related to the FM enhancement.

Such additional OV generation is confirmed by micro PL measurement, since OVs in SnO_2 samples dominantly determine their optical emission around 500-600 nm [21]. As shown in Fig. 4, the intensity of 554 nm emission of $Sn_{0.982}Cr_{0.018}O_{2-\delta}$ is much stronger than that of pure SnO_2, indicating that the much larger OVs concentration were generated due to the Cr doping.

However, it turns out that these additional OVs are generated at the inner of the the samples rather than at the surfaces. This can be seen clearly on XPS given in Fig. 2c, where the relative intensity of HBEC peak to LBEC peak determines the quantity of surface OVs [22]. As shown in Fig. 2c, the relative intensity of HBEC peak to the LBEC peak is 0.362 and 0.358 for the SnO_2 and $Sn_{0.982}Cr_{0.018}O_{2-\delta}$ samples, respectively. The nearly same contribution of the HBEC peak for the two samples indicates that the Cr doping does not induce more surface OVs. Note that, as the penetration depth of Mg Kα XPS is several nanometers, the measurement of XPS indicates the surface proporties of samples, whereas the PL measurement provides the optical properties of the whole sample. The difference between the PL and XPS measurement on our samples indicates that the substitution of Cr^{3+} for Sn^{4+} does not create OVs on the surface, but at the inner of samples. As surface OVs contribute to the FM of the pure SnO_2 nanowires [9], our observations imply that Cr doping does not tune the FM of the pure SnO_2 nanowires by introducing surface OVs.

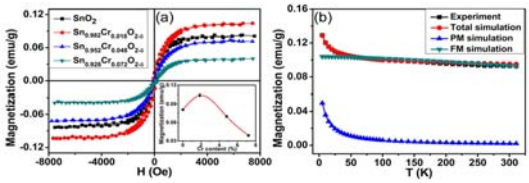

Figure 3. (a) Magnetic hysteresis loops of $Sn_{1-x}Cr_x O_{2-\delta}$ nanowires with x=0–0.072 measured at RT, the inset shows the V content dependence of the magnetization. (b) Temperature dependence of the magnetization for $Sn_{0.982}Cr_{0.018}O_{2-\delta}$ nanowires.

In this case, we prefer to explain the enhanced FM with the Cr doping in the framework of the bound magnetic polaron (BMP) model. Recent studies have shown a direct dependence of ferromagnetic ordering on the OVs concentration in some dilute magnetic semiconductor systems [2-4], where A BMP mediated exchange interaction was suggested as responsible for magnetic ordering. A BMP is an oxygen vacancy with a trapped electron. This trapped electron occupies an extended orbital state that overlaps with the *d* shells of several TM ions nearby. Since the OVs arise naturally to ensure charge neutrality when a trivalent ion is substituted in SnO_2 and the Cr^{3+} is in $3d^3$ spin state, they would have the unoccupied minority spin orbitals available for exchange with the trapped electron. The trapped electron will align in an antiparallel configuration with the individual dopant ion spins. This leads to an effective ferromagnetic coupling between coupled dopant ions. The greater density of OVs yields a greater overall volume occupied by BMPs, thus increasing their probability of overlapping more Cr ions into the ferromagnetic domains and enhancing FM. On the other hand, our experiment shows that the magnetization drops with increasing Cr content for the samples with x > 0.018 (Fig. 3, inset). This behavior can be explained that the further reduction will result from any antiferromagnetic Cr^{3+}–O^{2-}–Cr^{3+} superexchange interaction taken place within the nearest Cr^{3+} ions through O^{2-} ions.

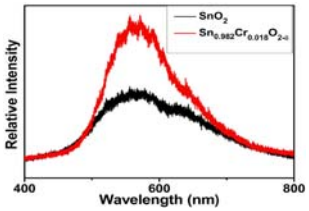

Figure 4. RT micro PL spectra of SnO_2 and $Sn_{0.982}Cr_{0.018}O_{2-\delta}$ nanowires taken at RT.

To further confirm the coexistence of ferromagnetic and antiferromagnetic coupling, the temperature dependence of magnetization was measured from 5 to 300 K in a 5 kOe field for $Sn_{0.982}Cr_{0.018}O_{2-\delta}$ nanowires (Fig. 3b). With increased temperature, the curve shows a rapid decay of magnetization at low temperature region, after which the magnetization declines gradually and does not go to zero at 300 K, indicating a paramagnetic phase mixed with a ferromagnetic phase for the sample. The PM comes from the magnetic moments of isolated Cr ions which are not bounded into magnetic polarons and hence do not exhibit ferromagnetic behavior. Based on these analyses, we can describe the *M-T* curve as a combination of the $T^{3/2}$ law of saturation magnetization for FM phase and a Curie–Weiss law for PM phase, given by the following equation: [23]

$$M = M_0(1 - BT^{3/2}) + CH/(T - P) \qquad (1)$$

where M_0 is the saturation magnetization at T = 0K, B is a constant, C is the curie constant, P is the Curie–Weiss temperature, and H is the applied magnetic field during measurement. In Fig. 3b, the ferromagnetic part, the paramagnetic part, and the total Ms-T curve simulated by equation (1) are plotted separately. It is seen that the simulated Ms-T curve agrees very well with the experimental results. Fitting the experimental data, we obtained P = -7.9. The negative P value implies the weak antiferromagnetic interaction existing in the samples, which is likely to be responsible for the magnetization decrease with increasing Cr content.

4 CONCLUSIONS

We have synthesized undoped SnO_2 and Cr-doped SnO_2 nanowires with RT FM using a catalyzer-assisted CVD method. 1.8 at.% Cr doping significantly enhances the magnetization, implying that a TM doping does play an important role in introducing FM. We suggest that the in intrinsic FM arises from (i) the surface OVs in the SnO_2 lattice, (ii) the ferromagnetic coupling between the unpaired 3*d* electrons of Cr as a result of hybridization between the 2*p* states of O with the 3*d* state of the dopant (i.e. BMP model). Therefore, both the OVs and the Cr dopants are supposed to be equally important to induce FM of SnO_2.

REFERENCES

[1] Y. Matsumoto, M. Murakami, T. Shono, T. Hasegawa, T. Fukumura, M. Kawasaki, P. Ahmet, T. Chikyow *et al.*, Science, 291, 854, 2001.
[2] M. Venkatesan, C.B. Fitzgerald, J.G. Lunney, J.M.D. Coey, Phys. Rev. Lett. 93, 177206, 2004.
[3] N.H. Hong, J. Sakai, W. Prellier, A. Hassini, A. Ruyter, F. Gervais, Phys. Rev. B 70, 195204, 2004.
[4] S.B. Ogale, R.J. Choudhary, J.P. Buban, S.E. Lofland, S.R. Shinde, S.N. Kale, V.N. Kulkarni, J. Higgins *et al.*, Phys. Rev. Lett. 91, 77205, 2003.
[5] M. Venkatesan, C.B. Fitzgerald, J.M.D. Coey, Nature 430, 630, 2004.
[6] N.H. Hong, J. Sakai, N. Poirot, V. Brizé, Phys. Rev. B 73, 132404, 2006.
[7] S.D. Yoon, Y. Chen, A. Yang, T.L. Goodrich, X. Zuo, D.A. Arena, K. Ziemer, C. Vittoria, V.G. Harris, J. Phys.: Condens. Matter 18, L355, 2006.
[8] N.H. Hong, J. Sakai, V. Brizé, J. Phys.: Condens. Matter 19, 036219, 2007.
[9] L. Zhang, S.H. Ge, H.X. Zhang, Y.L. Zuo, J. Nanosci. Nanotechnol. 10, 2010, in publish.
[10] N.H. Hong, E. Chikoidze, Y. Dumont, Physica B 404, 3978, 2009.
[11] Q.Y. Xu, H. Schmidt, S.Q. Zhou, K. Potzger, M. Helm, H. Hochmuth, M. Lorenz *et al.*, Appl. Phys. Lett. 92, 082508, 2008.
[12] M. Kapilashrami, J. Xu, V. Ström, K.V. Rao, L. Belova, Appl. Phys. Lett. 95, 033104, 2009.
[13] G.Z. Xing, J.B. Yi, D.D. Wang, L. Liao, T. Yu, Z.X. Shen, C.H.A. Huan, T.C. Sum, J. Ding, T. Wu, Phys. Rev. B 79, 174406, 2009.
[14] X.F. Duan, C.M. Lieber, Adv. Mater.12, 298, 2000.
[15] H. Takeuchi, M. Arakawa, J. Phys. Soc. Jpn. 52, 279, 1983.
[16] L. Yan, J.S. Pan, C.K. Ong, Mater. Sci. Eng. B 128, 34, 2006.
[17] G. Tyuliev, S. Angelov, Appl. Surf. Sci., 32, 381, 1988.
[18] C. Xu, M. Hassel, H. Kuhlenbeck, H.J. Freund, Surf. Sci. 258, 23, 1991.
[19] N.J.C. Ingle, R.H. Hammond, M.R. Beasley, J. Appl. Phys. 89, 4631, 2001.
[20] A. Sundaresan, R. Bhargavi, N. Rangarajan, U. Siddesh, C.N.R. Rao, Phys. Rev. B 74, 161306, 2006.
[21] J.H. He, T.H. Wu, C.L. Hsin, K.M. Li, L.J. Chen, Y.L. Chueh *et al.*, Small 2, 116, 2006.
[22] M. Naeem, S.K. Hasanain, M. Kobayashi, Y. Ishida, A. Fujimori, S. Buzby, S.I. Shah, Nanotechnology 17, 2675, 2006.
[23] S.H. Liu, H.S. Hsu, C.R. Lin, C.S. Lue, J.C.A. Huang, Appl. Phys. Lett. 90, 222505, 2007.